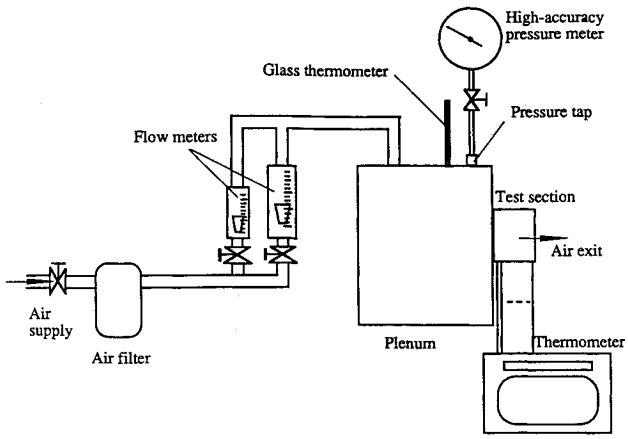

Fig. 5 Heat transfer experimental setup.

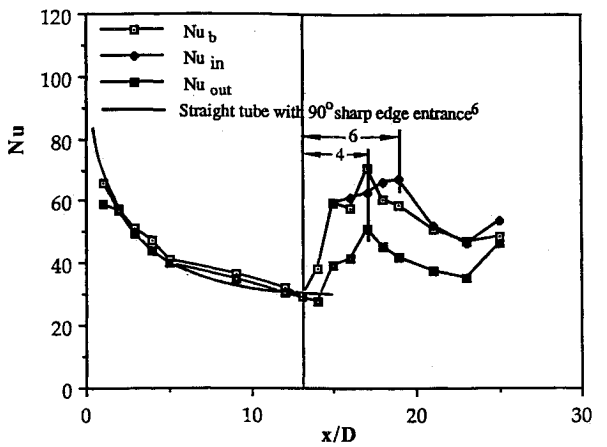

Fig. 6 Local Nusselt number for Re = 10,000; q = 1352.5 W/m^2.

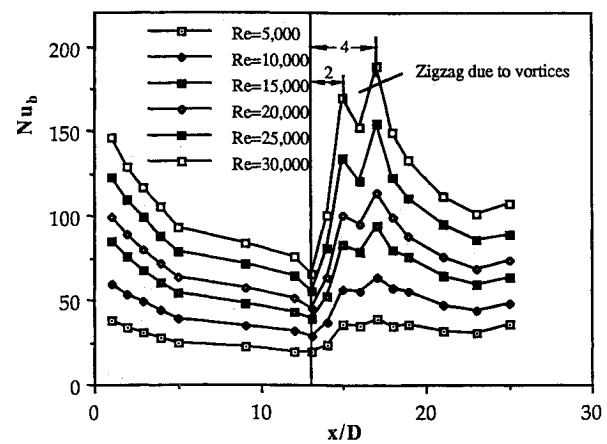

Fig. 7 Fluctuation of Nusselt number in the flow network.

region takes a different course depending upon the walls: the bottom (and top) and inner walls are characterized by a recovery in Nu beginning at the midway plane, but Nu of the outerwall continues to slide with x/D. In the fourth flow (final centrifugal) regime, all four walls undergo a significant heat transfer enhancement immediately after the intersection zone, reaching a maximum, followed by a decline toward the duct exit. However, one special event is seen to occur near the duct exit. This appearance of the thermal exit effect brings the number of thermal flow regimes in the flow network to five. Note that the monotonically decreasing line represents the Nu performance in a straight tube with 90-deg sharp-edge entrance. It is superposed in the figure for comparison. One additional feature in the fourth thermal flow regime is a zigzag in the Nu vs x/D curves around two to four times d downstream of the midway plane (i.e., flow intersection center) as seen in Fig. 7. The fluctuation of the Nusselt number of the bottom wall (Nu_b) is enhanced by increasing the Reynolds number. It can be explained by the action of vortices existing in this region. The same effects of the Reynolds number on the local Nusselt number also occurred on the inner and outer walls (not shown). However, the zigzag in Nu_{in} vs x/D curves is not so evident, and the heat transfer augmentation is caused by the flow impact on the right wall.

Conclusions

Thermal and hydrodynamic behavior in flow networks have been brought to light. Discussion is based upon equal flow rates in both ducts and the intersection angle of 60 deg which provides the optimal intersection pressure loss. It is disclosed that the formation of a flow divider in the intersection zone results in each stream following a curved flow path, shifting from the left to the right ducts and vice versa. The effect of a centrifugal force is therefore brought into play in the flow network. Four hydrodynamic flow regimes are identified through flow visualization, LDV and pressure measurements. The mechanisms of heat transfer in each of these four flow regimes are uniquely different, with an additional feature of thermal exit effect near the duct outlet.

References

[1]Zhang, N., Yang, W.-J., Xu, Y., and Lee, C. P., "Flow Characteristics in Flow Networks," *Experiments in Fluids*, Vol. 14, 1993, pp. 25–32.

[2]Zhang, N., Yang, W.-J., Xu, Y., and Lee, C. P., "An Application of Hydrogen Bubble Method to Flow Networks," *Flow Visualization VI*, edited by Y. Tanida and H. Miyashiro, Springer-Verlag, Berlin, 1992, pp. 90–96.

[3]Zhang, N., Yang, W.-J., and Lee, C. P., "Local Heat Transfer in Flow Networks," *Transport Phenomena Science and Technology*, Higher Education Press, Beijing, China, 1992, pp. 296–301.

[4]Umeda, S., and Yang, W.-J., "Mechanics and Correlations of Flow Phenomena in Intersecting Ducts," *Experiments in Fluids* (submitted for publication).

[5]Bunditkul, S., and Yang, W.-J., "Laminar Transport Phenomena in Parallel Channels with a Short Flow Construction," *Journal of Heat Transfer*, Vol. 101, No. 2, 1979, pp. 217–223.

[6]Mills, A. F., "Experimental Investigation of Turbulent Heat Transfer in the Entrance Region of a Circular Conduct," *Journal Mechanical Engineering Science*, Vol. 4, No. 1, 1962, pp. 63–77.

AlCl Absorption Feature in Solid Rocket Plume Radiation

W. K. McGregor,* J. A. Drakes,† K. S. Beale,‡ and F. G. Sherrell‡
Sverdrup Technology, Inc.,
Arnold Air Force Base, Tennessee 37389

Introduction

WHEN a high resolution ultraviolet scanning monochromator is pointed normal to the axis of an exhaust plume

Presented as Paper 92-2917 at the AIAA 27th Thermophysics Conference, Nashville, TN, July 6–8, 1992; received Aug. 7, 1992; revision received Dec. 10, 1992; accepted for publication Dec. 15, 1992.

*Senior Technical Specialist, AEDC Group, Arnold Engineering Development Center. Associate Fellow AIAA.

†Physicist, AEDC Group, Arnold Engineering Development Center. Senior Member AIAA.

‡Engineer, AEDC Group, Arnold Engineering Development Center.

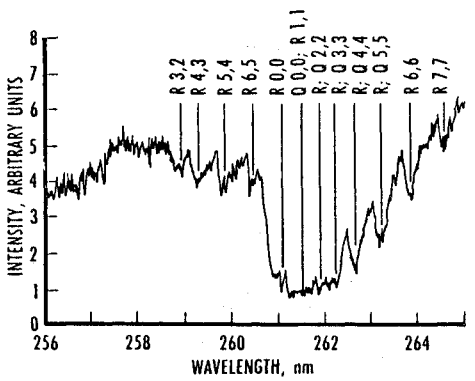

Fig. 1 High resolution UV spectra from solid-propellant rocket motor plume.

from an aluminized solid-propellant rocket motor being fired in an altitude test cell, the spectra shown in Fig. 1 results. The continuum on either side of the feature at 262 nm and the thermal behavior of the radiation in the visible and infrared regions suggests that the feature is due to absorption of a gaseous specie. A quick examination of the predicted products of combustion of ammonium perchlorate with aluminum and hydrocarbon solids, along with a trip through Pearce and Gaydon's[1] atlas of spectra, reveals that the most likely absorber is aluminum chloride (AlCl). Because of the small vibrational (~450 cm^{-1}) and rotational (0.25 cm^{-1}) constants of both AlCl states, a spectral resolution of about 0.1 nm was required to produce the band structure. The spectrum (Fig. 1) shows the expected structure and many of the bands listed in Pearch and Gaydon are identified.

AlCl Molecule

Aluminum chloride sublimates at temperatures above 460 K. A calculation of the plume properties using the JANNAF standard plume flowfield codes[2] shows that the solid temperatures are always above a minimum of about 600 K so that the AlCl is gaseous. Furthermore, the predicted mole fraction of AlCl is about 2.6%, and should follow the static pressure.

The molecular constants of the two electronic states, $A\,^1\Pi$ and $X\,^1\Sigma$, have been measured by several investigators and are reported critically by Huber and Herzberg.[3] The values are for $AlCl^{35}$, although $AlCl^{37}$ also naturally occurs; these two isotopes occur in the ratio 75.5:24.5. The relatively small vibrational constant of the ground state (480 cm^{-1}) leads to a vibrational-rotational fundamental at a wavelength of about 21 μm. (Observation of this LWIR emission band from rocket plumes has not been reported.) The constants of the $X\,^1\Sigma$ state have been remeasured recently in the infrared bands, and improvements in accuracy have been reported. These data will be introduced subsequently. The rotational constants for this closely packed molecule are also quite small (~0.254 cm^{-1}), and the overlapping branches make resolution of the lines near impossible.

The molecular constants for the $A\,^1\Pi$ state used in this state were taken from Huber and Hertzberg.[3] The vibrational correction to the rotational constant given as footnotes in Ref. 3 are a necessity for proper modeling of this band. Also, because of the small values of B_e, rotational quantum numbers out to at least 100 must be used at the temperatures of interest. For the ground electronic state, the latest reported measurements[4] use the Dunham expression[5] for the sum of the vibrational and rotational energy

$$T_{vJ} = \sum_{lm} Y_{lm}\left(v + \frac{1}{2}\right)^l [J(J+1)]^m \qquad (1)$$

These data were used as an alternate to the older Huber and Hertzberg[3] constants in an attempt to fit predicted and measured spectra more closely.

Radiative Transfer Model

The preliminary model adopted for this study is illustrated in Fig. 2. It is supposed that the core of solid particulates provides a continuum source for transmission through a layer of gas containing the absorbing AlCl. The continuum radiation from the particulates was curve fit by joining the spectra at both extremes of the absorption feature and served as a source for the absorption calculations. The gas layer was considered uniform for these preliminary calculations, with temperature and number density as parameters. The absorption spectra were modeled as Voigt lines with the spectrometer triangular slit function considered to be much greater than a linewidth.

A complete solution to the monochromatic radiative transfer equation is desired. The equation is written

$$\frac{dI_{\bar\nu}}{dx} = S_E N_{TOT} L_{\bar\nu} - S_A N_{TOT} L_{\bar\nu} I_{\bar\nu} \qquad (2)$$

where

N_{TOT} = total number density of emitter/absorber
$L_{\bar\nu}$ = a line shape function
S_E = molecular emission strength
S_A = molecular absorption strength
$I_{\bar\nu}$ = spectral radiance [i.e., $W/(sr\text{-}cm^2\text{-}cm^{-1})$] at wave number $\bar\nu$
x = spatial coordinate within the media

The boundary condition at $x = 0$ is given in this case by the fit to the continuum spectra, neglecting the AlCl absorption feature; i.e., the continuum background.

Conceptually, the calcuation involves three steps:

1) Determine the positions of all spectral lines. Determine the AlCl emission and absorption strengths for each line, based on rotational and vibrational temperature. This yields a spectral line atlas of line strengths at the line center wave number for all lines.

2) Given S_A, S_E, and N_{TOT}, solve Eq. (2). Here, only one zone is considered, so that integration of Eq. (2) is simplified.

3) Convolve the result of step 2 for each line with spectrometer reponse function. In this case a triangular slit function suffices, since the actual line width is much smaller than the instrument monochromatic response function.

Part 1

The strength of each emission line is given by

$$S_E = \frac{hc\bar\nu}{4\pi} A_{v'v''} \frac{S_{J'J''}}{2J'+1} \chi(A, v', J') \qquad (3)$$

where

$A_{v'v''}$ = Einstein coefficients[6]
$S_{J'J''}$ = Honl-London factors[5]
$\bar\nu$ = wave number
$\chi(A, v', J')$ = fractional population of the $A\,^1\Pi$ state for the v' and J' level, normalized by the partition function

$$\chi(A, v', J') = \frac{g_{Av'J'} \exp[-(hc/kT)E(A, v', J')]}{\sum_{\substack{\text{all}\\ \text{states}}} g_i \exp[-(hc/kT)E_i]} \qquad (4)$$

where g_i is the degeneracy factor of the given state.

The absorption strength is similarly given by

$$S_A = h\bar\nu B_{v'v''} \frac{S_{J'J''}}{2J''+1} [\chi(X, v'', J'') - \chi(A, v', J')] \qquad (5)$$

with the Einstein B coefficient as

$$B_{v'v''} = 1/(8\pi hc\bar\nu^3) A_{v'v''} \qquad (6)$$

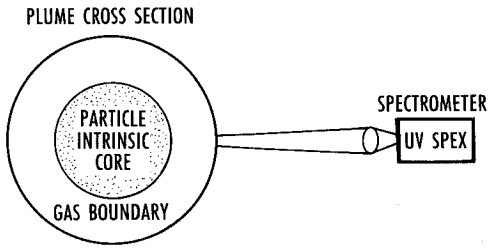

Fig. 2 Physical model of solid-propellant rocket motor plume UV spectral measurement experiment.

The band strength (or lifetime) of the AlCl $A^1\Pi \rightarrow X^1\Sigma$ (0, 0) transition has been measured[7] to be 6.4×10^{-9} s, where no effort was made to separate the two isotopic states. The relative band strengths were calculated by Langhoff and Bauschlicher[6] from first principles. They are given as Einstein coefficients and the relatively strong values for the $\Delta v = 0$ sequence indicate that these will be the most evident in the structure, which was also reported in the experimental analyses.[1] These calculations of band transition probabilities were made for $Al^{35}Cl$ with the assumption that the results are the same for $Al^{37}Cl$.

Energies of excited electronic state are given by the usual form in terms of the vibrational quantum number v, the rotational quantum number J, and the electronic angular momentum quantum number Λ

$$E(v, J) = T_e + G(v) + F_v(J) \tag{7}$$

where T_e is electronic state energy and $G(v)$ is the vibrational state energy given by

$$G(v) = \omega_e(v + \tfrac{1}{2}) - \omega_e x_e(v + \tfrac{1}{2})^2 + \omega_e y_e(v + \tfrac{1}{2})^3 \tag{8}$$

and F_v is the rotational energy given by

$$F_v(J) = B_v[J(J + 1) - \Lambda^2] - D_v[J(J + 1) - \Lambda^2]^2 \tag{9}$$

with

$$B_v = B_e - \alpha_e(v + \tfrac{1}{2}) + \alpha'_e(v + \tfrac{1}{2})^2 + \alpha''_e(v + \tfrac{1}{2})^3$$

$$D_v = D_e + \beta_e(v + \tfrac{1}{2})$$

For mass $Al^{37}Cl$ all constants are modified by the ratio $\rho = \sqrt{35/37}$

$$B_e^{(37)} = B_e^{(35)}\rho^2$$

$$\alpha_e^{(37)} = \alpha_e^{(35)}\rho^3$$

With the transition energies defined, line positions are obtained by subtraction

$$\bar{v} = E(A, v', J') - E(X, v'', J'')$$

A line atlas is built up from these expressions for v', v'' out to 8, and J', J'' out to 200 for both isotopes.

Part 2

The line-by-line model then solves Eq. (2) for each line in the atlas. A Voigt profile for each line is assumed. The S_E and S_A are calculated at 10 spectral frequencies between spectral lines by summing contributions of all relevant lines at that position. Here v', v'' out to 8, and J', J'' out to 200 are used to generate a large number of stored numbers. Thus, for 20,000 spectral lines, 200,000 radiances and transmittances are generated. The program also does spatial integration, although for this use (1 zone), this is trivial.

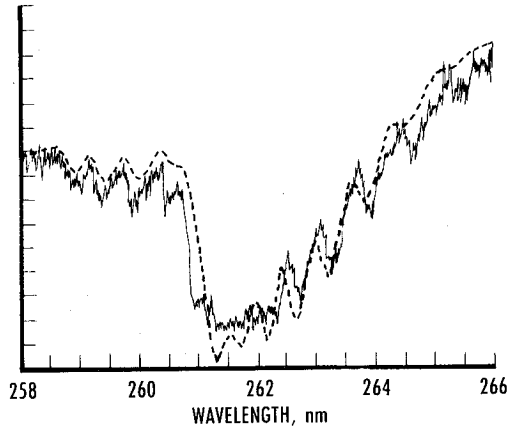

Fig. 3 Comparison of computed with measured spectra of SRM plume radiation at "best fit" conditions.

Part 3

The spectrometer is modeled by a triangle function of 2 Å full width at half-maximum. The convolution of the integral

$$H(\bar{v}) = \int I(\bar{v} - x)S(x)\, dx$$

is done numerically using the trapezoid rule, where $H(\bar{v})$ represents the instrument reading at $\bar{v}$, and $S(x)$ represents the instrument function.

Results

The approach taken was to vary the vibrational and rotational temperatures, the column density, and the column length in Eq. (2) until the closest fit to the experimental data was achieved. The temperature and pressure were varied about the predicted averages along the column, and the predicted mole fraction of AlCl was used initially. It was first necessary to calculate the constants accurately for each vibrational state of each of the isotopic molecules. This proved to be very sensitive in obtaining a fit to the vibrational bandheads. Then, the number of J values necessary to fit the absorption level was determined.

After a considerable number of iterations in parameter space, the best fit (Fig. 3) was obtained using the parameters:

Vibrational temperature	=	1000 K
Rotational temperature	=	1000 K
Number density	=	2.36×10^{16} cm^{-3}
Absorber path length	=	5 cm

Here, the spectal match is fair and the overall absorption matches satisfactorily, so that continued iteration appears unwarranted.

The final result is reasonable. Because of the high particle temperature, it is not surprising to have a gas temperature somewhat larger than predicted (1000 vs 800 K predicted). Also, because of small particles in the outer gas flow, it is not surprising that the radiation from the gas layer masks the absorption at the deepest absorption frequency. One might expect that an arbitrary shift of the wavelength for the experimental data would produce a better fit. But, attempts to make this match were only marginally successful. It must also be noted that the simple physical model of Fig. 2 cannot be correct, since the radiation is obviously extended and the AlCl exists all through the plume. However, the modeling brought assurance that the absorber was AlCl, and only a slight variation of temperature brought the model results very near the measured data.

Acknowledgments

The research reported herein was performed by the Arnold Engineering Development Center (AEDC), Air Force Ma-

teriel Command. Work and analysis for this research were done by personnel of Sverdrup Technology, Inc., AEDC Group, technical services contractor for the AEDC propulsion test facilities. Further reproduction is authorized to satisfy needs of the U.S. Government.

References

[1]Pearse, R. W. B., and Gaydon, A. G., *The Identification of Molecular Spectra*, Wiley, New York, 1963, p. 58.

[2]Dash, S. M., and Pergament, H. S., "A Computational System for the Analyses of Mixing/Chemical/Shock Processes in Supersonic Internal and Exhaust Plume Flowfields," AIAA Paper 80-1255, July 1980.

[3]Huber, K. P., and Herzberg, G., *Molecular Spectra and Molecular Structure*, Van Nostand Reinhold, New York, 1979.

[4]Bernath, P., "Molecular Constants of the $X^1\Sigma$ State of AlCl," *Journal of Molecular Spectroscopy* (to be published).

[5]Kovacs, I., *Rotational Structure in the Spectra of Diatomic Molecules*, Adam Hilger, London, 1969.

[6]Langhoff, S. R., and Bauschlicher, C. W., "Theoretical Studies of AlF, AlCl and AlBr," *Journal of Chemical Physics*, Vol. 88, No. 9, 1988, p. 5715–5725.

[7]Rogowski, D. F., and Fontijn, A., "The Radiative Lifetime of AlCl $A^1\Pi$," *Chemical Physics Letters*, Vol. 137, 1987, p. 219.

Parallel Processing Approach for Radiative Heat Transfer Prediction in Participating Media

C. Saltiel*
University of Florida, Gainesville, Florida 32611
and
M. H. N. Naraghi†
Manhattan College, Riverdale, New York 10471

I. Introduction

NUMERICAL analyses of radiative transfer in participating media can be very complex due to the long distance nature of radiative exchange. Computer simulations of practical situations often require both large computer memory and long calculation times. Serial processors have been used extensively for radiative analyses, but simulations can take hours on powerful machines like the CRAY Y-MP.[1]

The use of massively parallel machines, e.g., the single-instruction multiple-data (SIMD) connection machine (CM) with hypercube interprocessor connectivity, has proven very effective in simulating large complex systems.[2] Calculations are performed concurrently on tens of thousands of processors, each associated with memories arranged for efficient processor-to-processor communication (in contrast to coarse parallelism, where typically between 2 and 64 processors share memory). In finite difference and finite-element computations, each processor is associated with one or more spatial nodes, allowing all calculations on the data to be carried out simultaneously. Along with the promise of substantial increases in computational speed, massive parallelism also favors simpler computational algorithms since programming is array oriented, as in FORTRAN 90.[3]

Received Nov. 16, 1992; revision received Jan. 26, 1993; accepted for publication Jan. 29, 1993.

*Assistant Professor, Department of Mechanical Engineering.
†Associate Professor, Department of Mechanical Engineering.

Radiative computations are particularly well-suited for parallel processing. Recently Howell[4] has reviewed the use of parallel computing for radiative transfer but did not address the use of massively parallel architectures. Coarse parallelism has been described for Monte Carlo radiative heat transfer on an eight-processor ETA-10.[5] Hanebutte and Lewis[6] used a CM-2 for simulating radiative transfer in a two-dimensional enclosure via the discrete ordinates method. Other node-based radiative transfer solution techniques could also be programmed for parallel computation.

Typically, only a few hundred nodes are used for radiative transfer calculations in participating media, since fine-grained meshes are not required. Since current massively parallel architectures employ up to 2^{16} processors, a direct node-to-processor association would utilize only a small portion of the computing power available. Not only is it advantageous to maximally utilize each available processor, but algorithms with large memory requirements (in which array size exceeds the memory available to the processors) can be employed since many parallel machines have virtual processing ability, i.e., a single physical processor can act as multiple processors. A parallel computational scheme in which each processor is associated with radiative exchange between nodes, and not to the nodes themselves, would make full use of each processor. Such an approach corresponds to an exchange factor-(zonal-) based computation, where both direct and indirect radiative exchange between surfaces and volumes are calculated. The simplicity of this method as applied to parallel computing lies in the formulation of a unified matrix for total exchange factors. Within this context, parallel computations are programmed without regard to the dimensionality of the problem, so the same program can be used for one-, two-, or three-dimensional geometries. A unified matrix for zone-to-zone exchange factors has been formulated by Naraghi and Chung,[7] and could be applied directly to parallel computing. In this work we present a unified matrix formulation for node-to-node-based radiative exchange in isotropically scattering homogeneous media using the discrete exchange factor (DEF) method,[8] and compare computational implementation on serial and parallel computing machines.

II. Unified Matrix Formulation

The original formulation of the zone method, developed by Hottel and Sarofim,[9] offered an accurate and versatile method for radiative transfer analysis when it was first introduced in 1958. Since this time a number of modifications to this technique have been introduced, expanding the flexibility of the method for treating practical problems (including irregular geometries, inhomogeneous media, and anisotropic media), while concurrently simplifying programming. The literature contains many techniques for simplifying the zone method; a recent summary of some zone method extensions can be found in Ref. 10. For the sake of generalization, we refer to the zone method and its modifications as "exchange factor" methods, since radiative exchange between distinct regions can be expressed in terms of exchange factor matrices. This is an attractive feature of the exchange factor approach for massively parallel computing, since each matrix element can be associated to a processor.

A number of formulations have been proposed for exchange factor matrices. Noble[11] introduced an explicit matrix formulation for the zone method which significantly simplified programming. Further reducing programming, Naraghi and Chung[7] formulated a unified total exchange area matrix $\overline{ZZ}$ based on Markov chain theory

$$\overline{ZZ} = AB[B - \overline{zz}R]^{-1}\overline{zz}A \tag{1}$$

where

$$\overline{zz} = \begin{bmatrix} \overline{ss} & \overline{sg} \\ \overline{gs} & \overline{gg} \end{bmatrix} \tag{2}$$